Mixing Enhancement in Chemical Lasers, Part I: Experiments

Richard J. Driscoll*
Bell Aerospace Textron, Buffalo, New York

Nonreacting and reacting flow visualization experiments were used to demonstrate the ability of a new supersonic nozzle design (called the ramp nozzle) to accelerate mixing in a deuterium floride chemical laser via the reactant surface stretching mechanism. Unlike trip nozzles, which use inert gas injection to cause reactant surface stretching, the ramp nozzle causes a similar effect through its geometry without gas injection. The results from laser-induced fluorescence experiments indicate the ramp nozzle design produces a factor of two increase in the reactant interface length within about a centimeter of the nozzle exit. A side-by-side comparison in reacting flow of the ramp and gas trip nozzles suggest that both designs produce similar levels of mixing enhancement. These data are used to develop a phenomenological model for mixing enhancement in gas trip and ramp nozzles. This model describes a possible mechanism by which trip jets cause reactant surface stretching, indicates how the surface stretching rates can be calculated from the reactant nozzle geometry and flow conditions, and permits performance scaling laws consistent with the trip nozzle data to be derived.

Nomenclature

D = molecular diffusion coefficient
h_j = trip jet penetration height
$L(t)$ = reactant surface interface length
L_r = ramp or gas trip jet spacing
m_j = gas trip jet mass flow rate ($m_j = m_j^*$ when $h_j = w$)
p = laser cavity pressure
$s(t)$ = strain rate distribution function
s_r = $v_r/(2L_r)$, reference strain rate
T = temperature
t = x/u, axial flow time
u = axial velocity on reactant nozzle centerline
v = nozzle exit transverse velocity
v_r = $v_F + v_O$, reference transverse velocity
w = reactant nozzle half-width
x = axial distance
X, Y = axial and transverse distances for reactants to reach nozzle centerlines
α = transverse flow angle, $\sin^{-1}(v/u) = \tan^{-1}(Y/X)$
δ, δ^* = boundary-layer thickness, displacement thickness
Δ = $2(Dt)^{1/2}$ diffusion layer thickness
ψ = L/L_r, reactant interface extension ratio
θ_e, θ_w = effective and geometric nozzle wall angles

Subscripts

i = F (fuel nozzle) or O (oxidizer nozzle)
j = trip jet
r = reference value

I. Introduction

CONTINUOUS wave deuterium floride chemical lasers operating at high cavity pressures use trip nozzles to increase the reactant mixing rates and laser power.[1] When $p > 10$ Torr, diffusional mixing is slow compared with the lasing specie collisional deactivation rates[2] and the faster mixing produced by the trip jets is essential for achieving a high laser efficiency. In a trip nozzle, an inert gas is injected transversely between the reactant streams through discrete orifices located in the tips of the reactant nozzles. The trip jets are believed to increase the mixing rate by stretching the interface between the reactant streams.[3] The beneficial effect of reactant surface stretching on the mixing rates and laser power has been described in Ref. 3; however, the mechanism by which the trip jets produce such reactant surface stretching is not known. One purpose of this paper is to describe a possible mechanism and to show how the stretching rates can be calculated.

Trip nozzles have been very successful in increasing laser performance; but, they are costly and difficult to fabricate. In addition, the gas jets generate density disturbances in the laser cavity that have the potential for degrading the phase uniformity of the laser beam. Finally, the injected gas itself represents a barrier to mixing in that the laser fuel and oxidizer must diffuse through the inert trip jet gas before they can react. Therefore, it is desirable to develop new nozzle designs that generate significant levels of reactant surface stretching without gas injection. The primary purpose of this paper is to introduce such a nozzle design (the ramp nozzle) and to illustrate its characteristics using data from nonreacting laser-induced fluorescence flow visualization tests and from reacting flow infrared photography experiments. These experiments include a side-by-side comparison in reacting flow of the ramp and gas trip nozzles. The results from these experiments are used to develop a model for the surface stretching caused by the ramps and trip jets. This model leads directly to a strain rate distribution function that can be used with the theory of Ref. 3 to estimate the lasing characteristics of the gas trip and ramp nozzle designs. Herein, the simple consequences of the surface stretching model are outlined. More quantitative results including performance estimates using the laser scaling model from Ref. 3 and a comparison of results from a numerical aerokinetics code with laser gain data will be given in Part II of this paper.[4]

II. Nonreacting Flow Experiments

Figure 1 shows a photograph of one of the ramp nozzle arrays tested in our experiments. The geometry and dimensions of the nozzles in this array are shown in Fig. 2. The array consists of three fuel and two oxidizer nozzles in an alternating pattern. The overall dimensions of the array are 1.27×1.78 cm; its frontal area is 2.26 cm^2. There are no gas trip jets in this array; they have been replaced by ramps that extend backward from the nozzle exit plane into both the fuel and oxidizer nozzles. The top surfaces of the ramps are

Received June 3, 1985; revision submitted Nov. 12, 1985.

*Group Leader, Laser Fluid Mechanics. Member AIAA.

parallel to the nozzle centerlines and start just downstream of the nozzle throats. At the nozzle exit plane, the ramps extend more than half the distance across the nozzle exit dimension. For the design shown in Fig. 2, the ramp height to width ratio is 1.0 for the oxidizer nozzle and 0.60 for the fuel nozzle. The ramps in adjacent nozzles are offset from one another and spaced along 0.178 cm centers as shown in Fig. 2; this design duplicates the spacing and alternating pattern that has proved successful in trip jet nozzles. Without the ramps, the array shown in Fig. 2 is identical to the BCL-18 gas trip nozzle described in Ref. 5. The fuel nozzle has a nominal (no ramp) geometric area ratio of 10, while the value for the oxidizer nozzle is 20. The frontal area of the ramps at the nozzle exit plane cause a 22.3% blockage of the oxidizer nozzle and 21.4% of the fule nozzle, yielding geometric area ratios for the fuel and oxidizer nozzles in ramp nozzle array of 7.86 and 15.53, respectively

I_2 laser-induced fluorescence experiments[5,6] were conducted to visualize the flow structures created by the ramps. In these experiments, either the fuel or oxidizer stream is seeded with molecular iodine (I_2). The flow is then illuminated in a plane perpendicular to the axial flow direction using an argon ion laser operating on the 514.5 nm line. The laser pumps the I_2 molecule into an electronically excited state; as the excited I_2 decays, it fluoresces in the yellow region of the spectrum. Photography is used to record the I_2 emission and, thus, the location of the I_2 seeded material. Figure 3 shows the test configuration for these experiments. The I_2 fluorescence was recorded using a 35 mm camera and Kodacolor 400 film. A filter was placed in front of the camera to eliminate unwanted light from the laser pump beam. The camera was located 50 deg off the flow axis so that a frontal view of the flow could be photographed. A complete description of the experimental setup, procedures, and test equipment is given in Ref. 5.

Room temperature (298 K) helium was used as the test gas in both the fuel and oxidizer nozzles. At the nominal test conditions, the total mass flow rate through the three fuel and two oxidizer nozzles was 2.03 and 3.46 g/s, respectively. The total nozzle mass flux based on a 2.26 cm^2 flow area was 2.43 $g/s \cdot cm^2$; high-cavity-pressure chemical lasers typically operate in the mass flux range of 2-3 $g/s \cdot cm^2$. The fuel stream in a deuterium fluoride (DF) chemical laser is composed of a helium-deuterium mixture at about 600 K, while the oxidizer stream is composed of a mixture of gases with a molecular weight of about 13 and a total temperature (after combustor and nozzle heat losses) of about 1300 K. Except for the lower temperature, helium provides a good simulation of the laser fuel stream; the lower temperature leads to lower velocities at the nozzle exit; e.g., typical flow velocities in a chemical laser are about 2.2×10^5 cm/s, while the cold helium gives about 1.65×10^5 cm/s. The nozzle plenum pressures for the fuel and oxidizer streams scale as $p_0 = (m/A^*)(T_0/M_w)^{1/2}$. Since (m/A^*) is identical for the simulated and actual laser flows, differences in p_0 are due to changes in $(T_0/M_w)^{1/2}$. This results in the fuel and oxidizer stream plenum pressures being about 30 and 16% lower, respectively, in the simulated flow. Boundary layer calculations for the simulated flow indicate that the boundary-layer δ and displacement δ^* thicknesses for the fuel and oxidizer nozzles are $\delta/w = 0.33$ and 0.27 and $\delta^*/w = 0.26$ and 0.23, respectively (w is the appropriate nozzle half-width). Using the displacement thickness to correct the nozzle expansion gives estimates for the fuel and oxidizer nozzle exit pressures of about 1333 Pa (10 Torr); this value is essentially the same as that expected for an actual chemical laser operating at a mass flux of 2.0 $g/s \cdot cm^2$. The helium simulant, therefore, provides both the correct mass flux and nozzle exit pressure. As noted earlier, the flow velocities are lower in the simulated flow; the static temperatures in the cavity of the

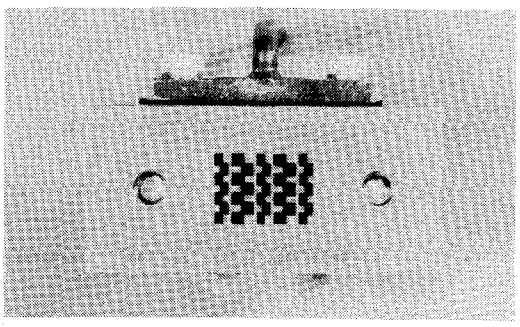

Fig. 1 Ramp nozzle used in the laser-induced fluorescence flow visualization experiments.

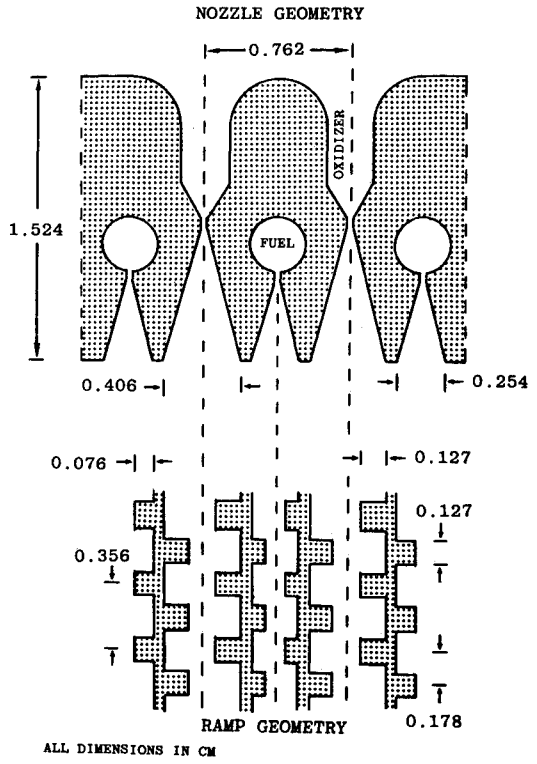

Fig. 2 Ramp nozzle geometry and dimensions.

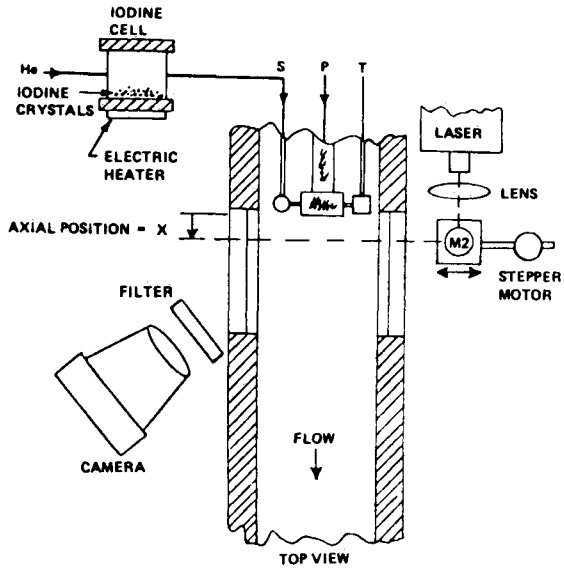

Fig. 3 Test configurations for laser-induced fluorescence flow visualization experiments.

simulated flow are also much lower than those in a real laser.

The lower static temperatures in the simulated flow are an advantage for the flow visualization experiments in that they inhibit molecular diffusion of the I_2-seeded material (since the diffusion coefficient D scales at $T^{5/3}$). For the conditions of our experiments, the static pressure and temperature in the cavity flow were estimated to be about 1333 Pa (10 Torr) and 50 K, respectively. At these conditions, the molecular diffusion coefficient for I_2 in helium is about 1 cm^2/s. The diffusive transport of I_2 from the seeded into the unseeded stream can be estimated from $\Delta = 2(Dx/u)^{1/2}$; with $u = 1.65 \times 10^5$ cm/s, this yields $\Delta = 0.007$ cm at $x = 2$ cm. For the nozzles shown in Fig. 2, the fuel and oxidizer nozzle half-widths are $w_F = 0.125$ and $w_O = 0.200$ cm, respectively, yielding $\Delta/w_F = 5.6\%$ and $\Delta/w_O = 3.5\%$ at $x = 2$ cm. In the near-nozzle region, diffusive transport of the I_2 should, therefore, be small and any movement of the I_2-seeded material will be primarily due to convective motion. The laser-induced fluorescence technique provides a simple means of visualizing this convective motion.

Figure 4 shows a series of photographs from the flow visualization experiments at the nominal test conditions. The flow through the two oxidizer nozzles was seeded with I_2. The light regions in Fig. 4 are due to I_2 fluorescence and they mark the material originating in the oxidizer stream. The dark regions mark the unseeded fuel stream material. At $x = 0$, the oxidizer stream has a crenellated shape that mirrors the ramp geometry. Downstream of the nozzle, oxidizer stream material flows into the base regions of the ramps in the adjoining fuel nozzles and consequently, the oxidizer stream is stretched into a set of long interconnected filaments. This filament structure is shown clearly in the $x = 0.76$ cm photograph. The fuel nozzle material is also distorted into a similar shape as can be seen by tracing the structure of the dark region. Fuel stream distortion is caused by the ramps in the oxidizer nozzles. The fuel stream structure was verified by conducting experiments in which the fuel rather than the oxidizer stream was seeded with I_2. The filaments from the two oxidizer nozzles reach the centerline of the intervening fuel nozzle at about $x = 0.90$ cm. Downstream of this junction point, the filaments approaching each other from opposite sides start to deflect and intertwine, so that at $x = 2.27$ cm, the flow has the appearance of small pockets of fuel stream material surrounded by filaments of the I_2-seeded oxidizer stream. The filaments at the outer edges of the nozzle block are seen to stretch more than those in the interior region, since their transverse motion is not retarded by filaments approaching from the opposite side; this effect is particularly clear in the $x = 1.52$ cm photographs.

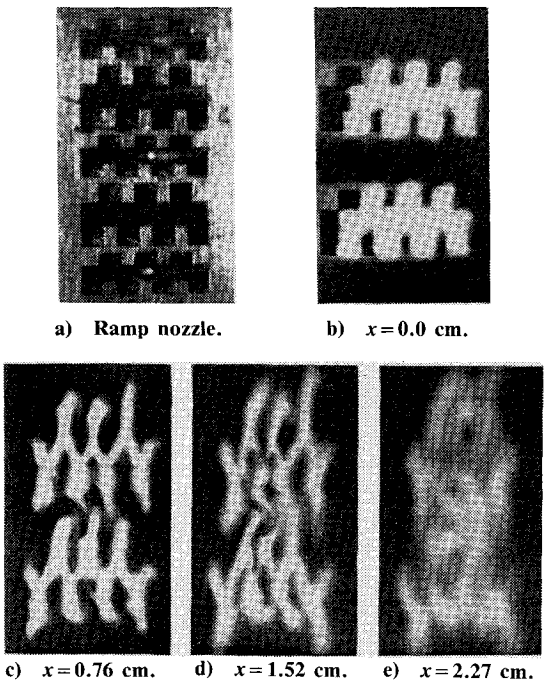

a) Ramp nozzle. b) $x = 0.0$ cm. c) $x = 0.76$ cm. d) $x = 1.52$ cm. e) $x = 2.27$ cm.

Fig. 4 Laser-induced fluorescence flow visualization of ramp nozzle flow patterns at nominal flowrates ($p = 10$ Torr); oxidizer nozzle seeded with I_2.

Flow visualization experiments were conducted at one-fifth the nominal flow rates to determine if the results shown in Fig. 4 were sensitive to the flow Reynolds number. For these tests, the nozzle exit pressure was about 400 Pa (3 Torr) and the nozzle boundary-layer scales are about a factor of two larger than those at the nominal flow conditions. The results from these low flow rate tests are given in Fig. 5 and they show that the reactant streams are distorted into a filament-type structure similar to that shown in Fig. 4. To first order, the lower Reynolds number and increased boundary-layer scales do not appear to change the character of the flowfield distortion caused by the ramps. The rate of distortion is, however, noticeably slower for the low flow rate tests as indicated by the longer distance required for the oxidizer stream filaments to reach the fuel nozzle centerline ($x = 1.20$ cm for the low flow rate tests vs $x = 0.90$ cm at the nominal flow rates).

III. Reacting Flow Experiments

Reacting flow experiments were conducted to verify that the ramp nozzle would provide mixing enhancement under actual chemical laser operating conditions and, also, to obtain a qualitative comparison between the gas trip and ramp nozzles. These experiments were conducted using a modified gas trip jet nozzle array (BCL-10). The BCL-10 nozzle array normally uses gas trip jets to provide mixing enhancement (see Ref. 7 for a complete description of BCL-10). One oxidizer nozzle in the array was modified to incorporate a set of ramps similar to those shown in Fig. 1. The ramp distribution was chosen to duplicate the gas trip jet pattern, i.e., the ramps on opposite nozzle sides were spaced along 0.178 cm centers. The ramps were 0.051 cm wide and 0.076 cm in height, i.e., a height/width ratio of 1.50.

A complete description of the test equipment, procedures, and experimental techniques for these reacting flow visualization experiments is given in Ref. 8. The experimental procedure is outlined below. The modified BCL-10 array was mounted in a laser cavity designed specifically to allow one to view from the side the reaction zones that form between the fuel and oxidizer streams. Photographs of the reaction zone structure in the laser cavity were taken with the laser operating at its nominal conditions. Typically, BCL-10 operates as a DF combustion-driven laser. The combustor reactants are C_2H_4 and NF_3, with helium as the diluent. The

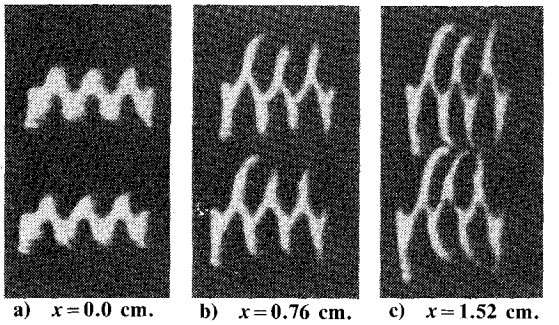

a) $x = 0.0$ cm. b) $x = 0.76$ cm. c) $x = 1.52$ cm.

Fig. 5 Laser-induced fluorescence flow visualization of ramp nozzle flow patterns at low flowrates ($p = 3$ Torr); oxidizer nozzle seeded with I_2.

combustor is run oxidizer rich to provide atomic fluorine (F) at the laser cavity inlet. The flow through the fuel nozzles is a mixture of helium and deuterium (D_2). The nominal operating mass flux for this laser is 2.0 g/s·cm^2 and the cavity inlet static pressure is about 1333 Pa (10 Torr).

The reaction zone structure was photographed using an infrared sensitive film (Kodak HIE-135) that records emissions in the 500-1000 nm region of the spectrum. Spontaneous emission at about 900 nm is produced by HF(3) via the $v=3\rightarrow0$ transition or DF(4) via the $v=4\rightarrow0$. Both HF(3) and DF(4) are produced when H_2 or D_2 react with F. Since the Einstein coefficient for the HF(3) transition is more than 200 times larger than that for DF(4), it was found[8] to be advantageous to seed the fuel nozzle flow with small amounts (0.1 g/s) of H_2 for all tests and then record the emission from the HF(3) transition. This procedure resulted in good definition of the reaction zone structure using short (30 s) photographic exposure times.

Figure 6a shows a typical result from the reacting flow experiments when the gas trip flow is off, while Fig. 6b shows the results from the same test with the gas trip flow at its nominal value of 4% of the total laser flow rate. The light regions in these photographs record the HF(3) $v=3\rightarrow0$ spontaneous emission and, therefore, mark regions of the flow where the laser fuel and oxidizer has both mixed and reacted. With the gas trip flow off, the reaction zone structure in all but the ramp nozzle shows a laminar mixing character with a thin well-defined flame starting at the junction of the fuel and oxidizer nozzles and then propagating slowly into the oxidizer stream (since the cavity flow is fuel rich). The laminar flame reaches the oxidizer nozzle centerline about 5 cm downstream of the nozzle exit plane. For the one oxidizer nozzle modified with the ramps, the reaction zone is seen to move rapidly into the oxidizer nozzle, reaching the nozzle centerline at about 0.8 cm from the nozzle exit plane.

Figure 6b provides a comparison of the gas trip and ramp nozzles when the gas trip flow is on and, to first order, the results suggest that the two mixing enhancement concepts are quite similar. Both the ramps and gas trips cause a rapid lateral transport of reactants, with the result that the reaction zone extends across the entire nozzle face when the flow is about 1.0 cm from the nozzle exit plane. The results in Fig. 6b also suggest that the lateral transport generated by the ramps is somewhat faster than that in the trip nozzle, since it is the ramp nozzle which first shows chemical reactions occurring on the oxidizer nozzle centerline.

The results in Fig. 6 demonstrate under realistic lasing conditions the strength of the lateral transport generated by the ramps and gas trip jets as compared to the slow diffusional motion of the laminar flame. For the ramp and gas trip nozzles, there is a factor-of-five shortening (from 5 to 1 cm) in the distance required for chemical reactions to occur on the oxidizer nozzle centerline. Figure 6 also demonstrates that the ramp nozzle will generate high levels of lateral transport under actual lasing conditions, just as it did in the nonreacting flow experiments shown in Figs. 4 and 5. Additionally, the side-by-side comparison of the ramp and gas trip nozzles shown in Fig. 6b implies that the ramp nozzle should provide mixing enhancement equal to that of the gas trip nozzles.

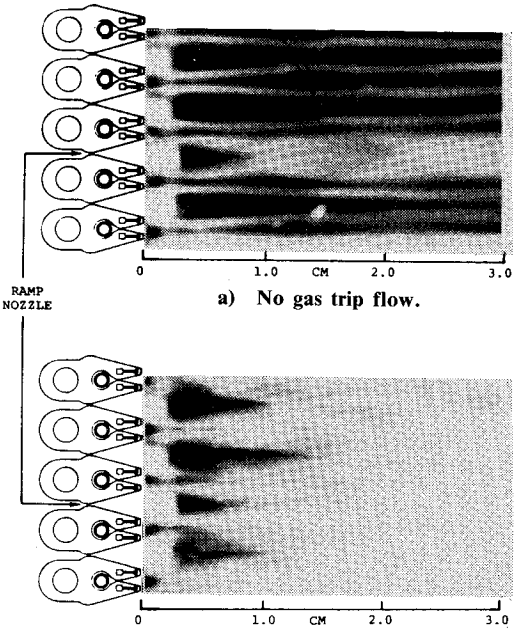

a) No gas trip flow.

b) Nominal gas trip flow.

Fig. 6 Flow visualization of ramp and gas trip nozzle reaction zones using infrared photography to record hydrogen fluoride spontaneous emission.

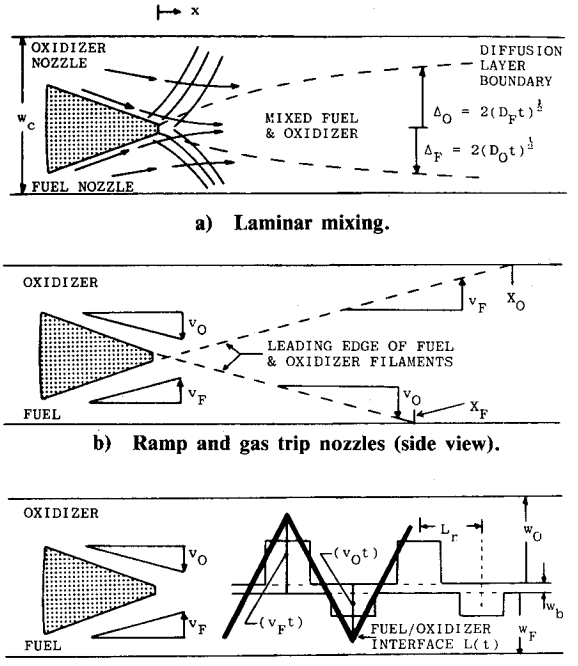

a) Laminar mixing.

b) Ramp and gas trip nozzles (side view).

c) Ramp nozzle (front view).

Fig. 7 Nozzle flow patterns.

IV. Mixing Enhancement Mechanism and Model

The data presented in Secs. II and III can be used to develop a phenomenological model for the surface stretching mechanism in ramp and gas trip nozzles. Let v_i, α_i, and u_i ($i=F$ or O) represent the nozzle exit transverse velocity, flow angle, and axial centerline velocity, respectively, for wedge nozzles these parameters are related by $v_i=u_i\sin\alpha_i$. The results in Fig. 4 show that the oxidizer nozzle filaments reach the fuel nozzle centerline at about $X_F=0.90$ cm. The lateral distance traveled by the oxidizer material is $Y_F=0.178$ cm (fuel nozzle half-width plus internozzle base width). This implies $\alpha_O=\tan^{-1}(Y_F/X_F)=11.2$ deg and, with $u_O=1.65\times10^5$ cm/s, that $v_O=3.2\times10^4$ cm/s. For the low flow rate tests shown in Fig. 5, $X_F=1.20$ cm; thus, $\alpha_O=8.4$ deg and $v_O=2.4\times10^4$ cm/s. The wall angle (θ_w) for this nozzle is 15 deg. The transverse flow angle α_i is less than θ_w and decreases as the nozzle flow rate decreases. This suggests that α and θ_w are related through the nozzle boundary-layer parameters. The effective expansion angle for a streamline in the neighborhood of the nozzle wall is θ_e, where $\tan\theta_e=(1-\delta^*/w)\tan\theta_w$. For the tests shown in Figs. 4 and 5, calculations using the method described in Ref. 9 indicate

that $\delta_O^*/w_O = 0.21$ and 0.41 and, therefore, that $\theta_e = 11.4$ and 8.8 deg, respectively, i.e., that $\alpha \approx \theta_e$. The lateral flow angle is approximately equal to the effective expansion angle of the source nozzle. This indicates that the nozzle wall angle and flow conditions, not the ramps or trip jets, define the magnitude of the transverse velocity.

Using $\alpha = \theta_e$, then the general expressions for v_i and α_i are

$$v_i = u_i \sin\alpha_i, \quad \tan\alpha_i = (1 - \delta_i^*/w_i)\tan\theta_{wi} \tag{1}$$

Equation (1) can be tested using the reacting flow data shown in Fig. 6. The BCL-10 nozzle array uses wedge-type reactant nozzles with $\theta_{wF} = 12$ deg and $\theta_{wO} = 15$ deg. For the ramp nozzle shown in Fig. 6, the axial distance required for chemical reactions to appear on the oxidizer nozzle centerline is about $X_O = 0.8$ cm; for the gas trip nozzles, the photographs indicate $X_O = 1.2$-1.4 cm. The distance required for chemical reactions to appear on the fuel nozzle centerline is $X_F = 0.3$-0.6 cm. These values for X_O and X_F are approximate due to the qualitative nature of the photographic data. For these reacting flow experiments, the nozzle exit flow properties are estimated from combustor, nozzle, and boundary-layer calculations as outlined in Ref. 10. The reactant stream widths Y_i just downstream of the nozzle exit are calculated to correct for static pressure differences that may exist at the nozzle exit. The results from these calculations give $Y_F = 0.058$ cm, $Y_O = 0.135$ cm, $\delta_F^*/w_F = 0.36$, and $\delta_O^*/w_O = 0.27$. Using Eq. (1) then yields $\alpha_F = 7.7$ deg and $\alpha_O = 11.1$ deg. X_i is calculated using $X_i = Y_i/\tan\alpha_j$; this gives $X_F = 0.30$ cm and $X_O = 1.0$ cm. The model, therefore, produces values of X_i that are in reasonable agreement with the photographic data in Fig. 6. Photographic data like those in Fig. 6 are given in Ref. 8 for the CL-XI gas trip laser nozzle array and calculations like those described above indicate Eq. (1) can also predict with reasonable accuracy the X_F and X_O values for this nozzle.

For a nozzle without ramps or gas trip jets, the fuel and oxidizer streams interact downstream of the nozzle exit plane as shown in Fig. 7a such that a weak compression system arises, canceling the transverse velocity components and turning both streams in the axial direction. In this situation, the reactant interface remains planar and there is no mixing enhancement. Now consider the ramp nozzle. Just downstream of each ramp, a wake will form with a length on the order of 5-10 times the characteristic ramp dimension.[11] For the nozzle shown in Fig. 1 with a ramp width and height of 0.13 cm, the axial extent of the wake should be on the order of 1.0 cm. The material within this wake consists of low-velocity recirculating gas, which should not prove to be a barrier to a high-velocity gas stream trying to penetrate from the underside. Thus, one can envision a situation such as that shown in Figs. 7b and 7c where the ramps create a series of wakes which do not block the transverse motion of the adjoining stream, but rather allow material from one reactant stream to move laterally in the other. The ramps and trip jets, therefore, appear to block the flow of the nozzle in which they are located, thereby creating a shadow into which material from the adjoining stream can move.

Th extent of the interface stretching can be estimated using the construction shown in Fig. 7c. The spacing between the ramps or trip jets is L_r; this distance also represents the undistorted (laminar mixing) length of the reactant interface for a scaleable segment of the flow. The transverse velocities at the nozzle exit planes are v_F and v_O. It is assumed that $u_F = u_O = u$ (a situation approximately satisfied in most chemical lasers) and that $t = x/u$. For simplicity, the interface between the reactant streams is assumed to remain linear during the stretching process, even though the results in Fig. 4 indicate that the shape of the interface is somewhat more complex; this assumption should provide a lower bound as the extent of surface stretching, since the more complex shapes will result in a longer reactant interface.

Using this linear interface model, the functional forms for $L(t)$, $\psi(t)$, and $s(t)$ are

$$L(t) = [L_r^2 + (v_F + v_O)^2 t^2]^{1/2} \tag{2a}$$

$$\psi(t) = L(t)/L_r = [1 + (2s_r t)^2]^{1/2} \tag{2b}$$

$$s(t) = (dL/dt)/L = 4s_r^2 t/\psi^2(t) \tag{2c}$$

The functions $s(t)$ and $\psi(t)$ are shown in Fig. 8; $s(t)$ has a maximum value equal to s_r at $t = (2s_r)^{-1}$. For $(s_r t) = 1$, $\psi = 2.24$ while for $(s_r t) = 5$, $\psi = 10.04$; these results indicate that high levels of surface stretching can be generated via the mechanism illustrated in Fig. 7c.

The results from this model can be checked against the data shown in Fig. 4. For these experiments $v_F = v_O = 3.2 \times 10^4$ cm/s. The ramp spacing is $L_r = 0.178$ cm, which yields $s_r = 1.80 \times 10^5$ s^{-1}. The axial velocity was estimated to be $u = 1.65 \times 10^5$ cm/s; thus, at $x = 0.76$ cm, $t = 4.6 \times 10^{-6}$ s, $(s_r t) = 0.83$, and Eq. (2b) gives $\psi = 1.94$. This value for ψ is in good agreement with the value of 2.0 estimated by measuring the interface length in Fig. 4.

Equation (2) cannot be used for the entire cavity flowfield. For example, consider the results shown in Fig. 4. If Eq. (2) is used to calculate L/L_r at $x = 1.52$ cm, then one obtains $\psi = 3.46$; this high value is not supported by measurements of the interface lengths using the results shown in Fig. 4. Further, consider the CL-XI laser.[8] At its normal operating conditions, characteristic values for u and s_r are 2×10^5 cm/s and 3.9×10^5 s^{-1}, respectively. With these values, Eq (2) implies $\psi = 19.5$ over the 5 cm distance representative of the lasing region for this nozzle. This nineteenfold surface extension level implies laser performance levels well in excess of those that are actually observed. Based on these examples, it is believed that there is a mechanism which reduces the surface extension rate in the downstream region of the laser cavity.

Figures 4 and 5 show that filaments moving in opposite directions interact with one another when they reach the intervening nozzle centerline, such that the filaments are deflected to form small entangled pockets of fuel and oxidizer. This interaction appears to reduce the transverse velocity that characterizes the stretching of the filaments and consequently reduces the reactant surface stretching rate. The ramp nozzle photographs, therefore, suggest that the cause of the reduction in the surface stretching rate is the interaction between oppositely directed filaments.

The model used to describe this filament interaction is as follows. At $x = X_F$, the oxidizer filaments collide on the fuel nozzle centerline; for $x < X_F$ the lateral velocity of the oxidizer filaments is v_O, while for $x > X_F$ this velocity is taken as ϵv_O, where ϵ is a small number on the order of 0.10 (see Ref. 4). Similarly, for $x < X_O$, the lateral velocity of the fuel

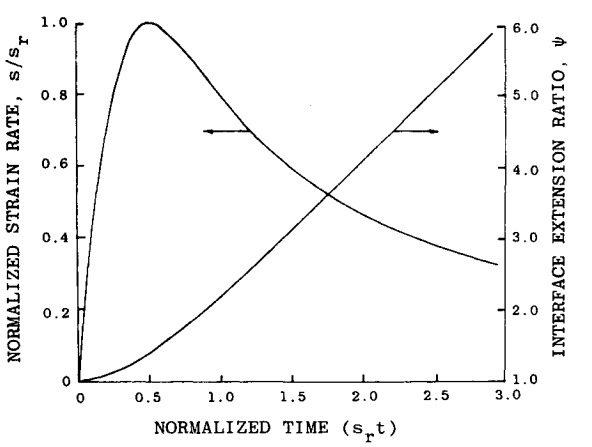

Fig. 8 Strain rate distribution function $s_r(t)$ and interface extension function $\psi(t)$ for ramp and gas trip nozzles in region 1.

filaments is v_F, while for $x>X_O$ this velocity is taken as ϵv_F. The parameter ϵ is assumed to be constant for $x>X_F$ and $x>X_O$. Since, in general, $X_F<X_O$, a three-region strain rate model will result. As an example, consider the situation where $X_F<X_O$; this is the case most commonly encountered in chemical lasers (e.g., see Fig. 6). It is simpler to use a time variable rather than distances to characterize flow through the cavity; let $t_1=X_F/u$, $t_2=X_O/u$, and $t=x/u$. In region 1 where the filaments are moving freely ($0<t<t_1$), the characteristic strain rate is s_r. Using the model illustrated in Fig. 7c, the results for $\psi(t)$ and $s(t)$ can be written as

Region 1

$$s_r=(v_F+v_O)/(2L_r)=v_r/(2L_r) \tag{3a}$$

$$\psi^2(t)=1+(2s_rt)^2 \tag{3b}$$

$$s(t)=4s_r^2t/\psi^2(t) \tag{3c}$$

In region 2 $t_1<t<t_2$, where the transverse velocity of the oxidizer filaments is (ϵv_O), the corresponding results are

Region 2

$$s_2=(v_F+\epsilon v_O)/(2L_r) \tag{4a}$$

$$\psi^2(t)=1+4[(s_r-s_2)t_1+s_2t]^2 \tag{4b}$$

$$s(t)=4s_2[(s_r-s_2)t_1+s_2t]/\psi^2(t) \tag{4c}$$

In region 3 ($t>t_2$) where the transverse velocities of the filament are (ϵv_F) and (ϵv_O), the model yields

Region 3

$$s_3=\epsilon s_r \tag{5a}$$

$$\psi^2(t)=1+[4(s_r-s_2)t_1+(s_2-s_3)t_2+s_3t]^2 \tag{5b}$$

$$s(t)=4s_3[(s_r-s_2)t_1+(s_2-s_3)t_2+s_3t]/\psi^2(t) \tag{5c}$$

The model outlined above can be used when $X_O<X_F$ by defining t_1, t_2, and s_2 as follows: $t_1=X_O/u$, $t_2=X_F/u$, and $s_2=(\epsilon v_F+v_O)/(2L_r)$.

To summarize, these are three elements in the mixing enhancement model for ramp and gas trip nozzles. The first element is generation of high transverse velocities by the reactant source nozzles. The second is flow blockage caused by the ramps or gas trip jets that allow lateral transport of the reactants to occur in their wakes. The third is a reduction in the lateral velocity of the filaments that occurs when opposing filaments interact. Each of these elements is an essential part of the overall model since each provides an explanation for part of the data described in Secs. II and III.

V. Discussion

The model outlined in Sec. IV cannot differentiate between ramp and gas trip nozzles. There are, however, some notable differences. For example, the gas jets form an inert gas layer between parts of the reactant streams. This gas layer retards molecular mixing and also causes density perturbations with the potential for degrading the phase uniformity of the laser beam. These two factors indicate possible advantage for the ramp nozzle. The gas trip jet approach does provide a means for continuously varying the degree of reactant surface stretching by changing the gas jet flow rate from zero (laminar mixing) to values on the order of 10% of the total laser flow rate. The ramps, on the other hand, cannot be "turned off," as is clearly illustrated in Fig. 6a.

Wilson[1] reports that trip nozzle power per unit area δ is relatively insensitive to reactant nozzle size. This result has yet to be explained satisfactorily; the laminar and turbulent mixing models of Mirels[2] and the correlation equation presented by Wilson[1] all indicate that $\delta\sim 1/w$, i.e., performance scales inversely with nozzle size. The surface stretching model from Sec. IV provides a possible explanation for the observed performance scaling.

For the scaling analysis, assume that laser power P is proportional to the reactant mixing rates and, therefore, to the length of the contact surface between the reactant streams (a more qualitative analysis is given in Ref. 4). Consider a scalable element of the flow bounded by the nozzle centerlines and the trip jets. The area of this element is $A=w_cL_r$, where $w_c=w_F+w_O+w_b$ is the centerline spacing of the nozzles (see Fig. 7). The contact surface length in the element is $L=\psi_rL_r$, where ψ_r is a constant reference value of the surface extension ratio. With $P\sim L$ and $\delta=P/A$, then to first order $\delta\sim\psi_r/w_c$. When no surface stretching occurs $\psi_r=1$ and $\delta\sim 1/w_c$, i.e., laminar mixing scaling[2] is recovered. A simple flowfield is assumed; let $v_F=v_O=v_r/2$, $u_F=u_O=u$, and $w_F=w_O$. This implies $X_F=u(w_F+w_b/2)\div v_O=X_O=X_r$ and that $t_r=X_r/u=w_c/v_r$. Further, let $\epsilon=0$; all surface stretching stops at $t=t_r$ and the surface extension ratio is constant and equal to $\psi_r=\psi(t_r)$ when $t>t_r$. From Eq. (3b), one has

$$\psi_r=(1+\mu)^{1/2},\ \text{where}\ \mu=(2s_rt_r)^{1/2}=(w_c/L_r)^2 \tag{6}$$

ψ_r represents the maximum value of surface extension ratio (when $\epsilon=0$) and it depends only on the nozzle geometry (L_r,w_c). Combining $\delta\sim\psi_r/w_c$ and Eq. (6) yields

$$\delta\sim(1+\mu)^{1/2}/w_c \tag{7a}$$

$$\delta\sim 1/L_r\ \text{for}\ \mu\gg 1 \tag{7b}$$

When $\mu\gg 1$, δ is independent of the nozzle size and depends only on the trip jet spacing. Wilson[1] indicates tests have been conducted on trip nozzles over the range $w_c=0.15-0.40$ cm ($\mu\approx$3-20 for $L_R=0.09$ cm). Figure 9 shows how the relative value of δ, calculated from Eq. (7a), varies with w_c over this range. The results indicate that a factor of 2.7 increase in w_c produces only a 12% decrease in δ; for $w_c\to\infty$, the asymptotic decrease in δ is only 14%. The performance scaling exhibited by the surface stretching model, therefore, appears to be consistent with data[1] showing that the trip nozzle performance is insensitive to the nozzle size.

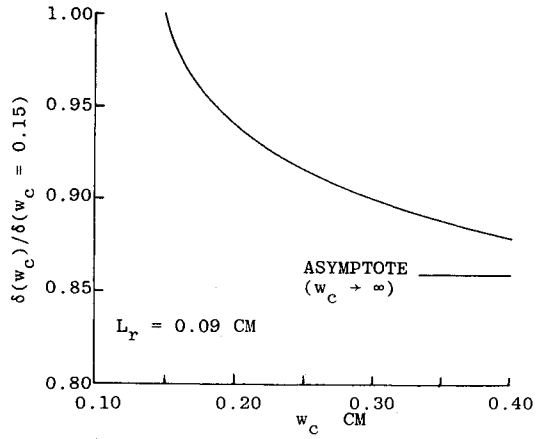

Fig. 9 Effect of nozzle scale on laser performance.

The effect of surface stretching can be viewed in a number of different ways. Let $\delta\sim 1/w_c$ represent the laminar mixing scaling law and $\delta\sim\psi_r/w_c$ the law for gas trip nozzles. Mixing across the reactant interface, whether stretched or not, is diffusional in both cases. A comparison of these two scaling laws, therefore, implies that gas trip nozzles, in effect, reduce the diffusional mixing scale from w_c to $w_c^*=w_c/\psi_r$. Another approach often used to describe gas trip laser flows is to assume the accelerated mixing can be modeled by increasing the molecular diffusion coefficient.[8,13] In a laminar flow, the characteristic diffusional mixing time for transverse scale w_c is $t\sim w_c^2/D$; if the transverse mixing scale is $w_c^*=w_c/\psi_r$, then the mixing time is $t\sim w_c^2/(\psi_r^2D)$. A comparison suggests that trip nozzles can be modeled approximately via a laminar mixing calculation using a molecular

diffusion coefficient which has been increased by a factor of ψ_r^2. For typical trip nozzles, $\psi_r^2 \approx 5$; therefore, the effect of the trip jets can be viewed as providing the equivalence of a fivefold increase in the diffusion coefficient. The diffusion coefficient multiplier (DCM) approach has proved to be quite successful in modeling trip nozzle data[8,13] and the discussion above indicates that the surface stretching model outlined herein not only provides a theoretical basis for the DCM approach, but also suggests that the value for the DCM is ψ_r and the DCM is a function of the nozzle geometry. A more quantitative description of the correspondence between the DCM and surface stretching model is given in Ref. 4.

Equation (6) implies that, when μ is large, δ is independent of w_c; thus, it is useful to examine the effects that would limit the size of the reactant nozzles. The model upon which Eq. (6) is based assumes that the gas trip jets penetrate to the reactant nozzle centerlines. Let h_j represent the lateral penetration of the trip jets and m_j the trip gas mass flow rate. Zukoski and Spaid[12] indicate that $h_j \sim m_j^{1/2}$; therefore, if one doubles the size of the reactant nozzles, the trip flow rate must increase by a factor of four in order for the jets to penetrate to the nozzle centerline. Typical nozzles have a trip gas mass flow rate that is 3-5% of the total flow; doubling nozzle sizes implies that trip flow rates of 12-20% would be needed. Injecting this much inert gas between the reactants will form a barrier that will slow diffusional mixing. This effect of the trip gas was neglected in the surface stretching model, since the amount of gas used is usually small. However, this will not be the case for large nozzles and, in trying to increase the nozzle size, it is believed that the performance limit occurs when the reduction in the diffusional mixing rate due to the inert gas layer is larger than the surface stretching effect of the jets. The ramp nozzle design may be more effective than the gas trip jets in large reactant nozzles since no gas injection is used.

It is known that laser performance is sensitive to trip jet penetration and this effect can be described by the model outlined in Sec. IV. Let m_j^* represent the trip flow rate required for the jets to penetrate to the nozzle centerlines, i.e., $h_j = w$ when $m_j = m_j^*$. When $m_j < m_j^*$, the lateral motion of the reactants stops after a distance h_j and the extent of surface stretching is found by replacing w_c in Eq. (6) with $(2h_j)$. Since $(2h_j) < w_c$, the extent of surface stretching is lower for incomplete penetration of the jets and, therefore, since $\delta \sim \psi / w_c$, the laser performance will be lower. When $h_j = 0$, then $\psi = 1$ and the mixing is laminar. When $m_j > m_j^*$, the jets penetrate to the nozzle centerline and the transverse motion of the reactants stops at the centerline due to the interaction of opposing gas jets; Eq. (6) then gives the extent of surface stretching. The performance appears to separate into two operational regimes depending on the trip flow rate. For $m_j < m_j^*$, the surface extension ratio and laser performance should both increase as m_j increases. For $m_j > m_j^*$, surface stretching is terminated with the interaction of the trip jets on the nozzle centerline and, since ψ is independent of trip flow rate in this regime, one also expects laser performance to show little sensitivity to m_j. Experimental data on trip nozzles show a rapid initial rise in laser power with trip flow rate followed by a plateau region where increasing trip flow further has relatively little effect; these results are consistent with those impled by the surface stretching model.

Finally, it should be noted that the surface stretching model outlined herein can be verified by a simple test. Equation (1) indicates that the lateral motion of the reactants is due to the transverse velocity at the nozzle exit plane. This implies that if the trip jets were placed at the exit of perfectly contoured nozzles with $\theta_w = 0$, the the transverse velocities would be zero and stretching of the type shown in Figs. 4 and 5 would not occur. Such a test could be used to verify the physical principles underlying this surface stretching model.

VI. Conclusions

Laser-induced fluorescence experiments demonstrated that the ramp nozzle increases the length of the interface between reactant streams in a chemical laser nozzle. Reacting flow photographic tests on a modified chemical laser nozzle array demonstrated the ramp nozzle at realistic laser conditions and also showed that the mixing enhancement processes in ramp and gas trip nozzles are similar. These data were used to construct a phenomenological model for mixing enhancement in chemical lasers. The elements of this model are: 1) the transverse velocity at the exit of the reactant nozzles generate lateral motion; 2) the ramps and trip jets block the nozzles flows so that lateral motion can occur in their wakes; and 3) lateral motion is stopped by incomplete trip jet penetration or by opposing filaments interacting at the reactant nozzle centerlines. While more data are needed to verify this model, the results derived from it appear to be consistent with available data. In particular, unlike earlier laminar and turbulent mixing models,[2] the surface stretching model indicates that the performance of a gas trip or ramp nozzle array will be relatively insensitive to the reactant nozzle size, in agreement with the data of Wilson.[1] A simple test of the model would be to examine the flow pattern caused by trip jets or ramps in nozzles with parallel outflow; if the model is correct, surface stretching such as that shown in Figs. 4 and 5 should not occur, since there is no traverse velocity component at the nozzle exit.

Acknowledgment

The work reported herein was sponsored under a Bell Aerospace Textron IR&D Program. A number of people have contributed significantly to the work reported herein; the contributions of C. E. Stricklin, G. W. Tregay, and A. A. Cenkner are gratefully acknowledged.

References

[1]Wilson, L. E., "Deuterium Fluoride CW Chemical Lasers," *Journal de Physique*, Colloque C9, Vol. 41, Nov. 1980, pp. C9.1-C9.8 (also AIAA Paper 76-344 by L. E. Wilson and D. L. Hook).

[2]Mirels, H., Hofland, R., and King, W. S., "Simplified Model of CW Diffusion-Type Chemical Laser," *AIAA Journal*, Vol. 11, Feb. 1973, pp. 156-164.

[3]Driscoll, R. J., "The Effect of Reactant-Surface Stretching on Chemical Laser Performance," *AIAA Journal*, Vol. 22, Jan. 1984, pp. 65-74.

[4]Driscoll, R. J., "Mixing Enhancement in Chemical Lasers, Part II: Theory," submitted to *AIAA Journal*.

[5]Cenkner, A. A. and Driscoll, R. J., "Laser-Induced Fluorescence Visualization on Supersonic Mixing Nozzles that Employs Gas Trips," *AIAA Journal*, Vol. 20, June 1982, pp. 812-819.

[6]Rapagnani, N. L. and Davis, S. L., "Laser Induced I_2 Fluorescence Measurements in a Chemical Laser Flowfield," *AIAA Journal*, Vol. 17, Dec. 1979, pp. 1402-1404.

[7]Cenkner, A. A., "Laser Doppler Velocimeter Measurements on Supersonic Mixing Nozzles that Employ Gas Trips," *AIAA Journal*, Vol. 20, March 1982, pp. 383-389.

[8]Driscoll R. J. and Tregay, G. W., "Flowfield Experiments on a DF Chemical Laser," *AIAA Journal*, Vol. 21, Feb. 1983, pp. 241-246.

[9]Driscoll, R. J., "Study of the Boundary Layers in Chemical Laser Nozzles," *AIAA Journal*, Vol. 14, Nov. 1976, pp. 1571-1577.

[10]Zelazny, S. W., Driscoll, R. J., Raymonda, J. W., Blauer, J. A., and Solomon, W. C., "Modeling DF/HF CW Lasers: An Examination of Key Assumptions," *AIAA Journal*, Vol. 16, April 1978, pp. 297-304.

[11]Chang, P. K., *Separation of Flow*, Pergamon Press, New York, 1970, Chaps. VII and X.

[12]Zukoski, E. E. and Spaid, F. W., "Secondary Injection of Gases into a Supersonic Flow," *AIAA Journal*, Vol. 2, Oct. 1964, pp. 1689-1696.

[13]O'Keefe, D., Sugimura, T., Behrens, W., Bullock, D., and Dee, D., "Comparison of LAMP and BLAZER Code Calculations with TRW CL-XV Measurements," *Optical Engineering*, Vol. 18, July-Aug. 1979, pp. 363-369.